http://dx.doi.org/10.5012/bkcs.2013.34.3.788

Development of Multi-sample Loading Device for TEM Characterization of Hydroxyapatite Nanopowder

Jong-Moon Lee,[†] Jung-Kyun Kim,[†] Jong-Man Jeong,[‡] Jin-Gyu Kim,[‡] Eunji Lee,[†] and Youn-Joong Kim[†,‡,*]

[†]*Graduate School of Analytical Science and Technology, Chungnam National University, Daejeon 305-764, Korea*
[*]*E-mail: y-jkim@kbsi.re.kr*
[‡]*Division of Electron Microscopic Research, Korea Basic Science Institute, Daejeon 305-333, Korea*
Received October 23, 2012, Accepted December 10, 2012

A shortcoming of using transmission electron microscopy (TEM) for structural analysis *via* electron diffraction is the relatively large error of the measurements as compared to X-ray diffraction. To reduce these errors, various internal standard methods from earlier studies have been widely used. We developed a new device to facilitate the application of internal standard methods in preparation of TEM grids used for nanopowder analysis. Through the application of a partial mask on the TEM grid, both the internal standards and the research materials can be loaded on the same grid. Through this process, we conducted a TEM analysis that compared synthetic hydroxyapatite (HAp) nanopowder to bone apatite from a bovine femur. We determined that the accuracy of the d-spacing measurements of the HAp and bone powders could be improved to better than 1% after statistical treatments of the experimental data. By applying a quarter mask, we loaded four different nanoparticles on a single TEM grid, with one section designated for the internal standard.

Key Words : Internal standard, Structure analysis, Multi-sample loading device, Transmission electron microscopy (TEM), Hydroxyapatite nanopowder

Introduction

Because nanotechnology is advancing at a fast-growing rate, it is increasingly important to analyze nanomaterials according to various physicochemical properties and conditions. Transmission electron microscopy (TEM) is one of the most widely used instruments to characterize nanomaterials. Through bright-field (BF), dark-field (DF), and high-resolution (HR) imaging, morphological analyses of nanomaterials can be conducted from the μm scale to atomic scale; also, through electron diffraction (ED), the crystal structure can be analyzed.[1-3] Additionally, qualitative and quantitative chemical analyses of nanomaterials are performed through energy dispersive spectroscopy and electron energy loss spectroscopy.[4,5]

However, TEM presents limitations for the structural analysis of materials *via* ED, because the errors in the experimental data are generally larger for ED than for X-ray diffraction (XRD).[6-8] The errors are derived from instrumental limitations (lens aberrations, unstable voltage and current, *etc.*), ultra-thin TEM samples (shape effect), dynamical scattering, and measurement errors in the diffraction data.[9,10] The method of using an internal standard has been widely applied to improve the accuracy and precision of ED analyses.[11] Some methods of using internal standards are described in the following: (1) installing two semi-circular grids clamped side-by-side in a TEM sample holder, where one side contains the sample and the other contains the standard; (2) stacking two separate grids (one with the sample and the other with the standard) on top of each other in a TEM sample holder; and (3) depositing the standard on one side of an amorphous carbon film, and the sample on the other side of the film on a single grid.[12] Unfortunately, all these methods have shortcomings. For the first and third cases of using two semi-circular grids and a single grid, respectively, TEM operations cannot be carried out simultaneously on both the standard and research samples. For the second case of stacking two grids, the quality of the image and ED pattern both decrease owing to the increase in electron scattering from the standard materials.[13] Additionally, the reliability of the TEM data from the application of these methods largely depends on the skills of the operator.[12]

In this study, we developed a multi-sample loading device that resolves the shortcomings of the conventional internal standard methods. The device has four separate sections where different samples can be independently loaded, thus, allowing us to analyze different samples simultaneously. By using this device, we conducted TEM characterization of synthetic hydroxyapatite (HAp) nanopowder and bone powder from a bovine femur.

Experimental Methods

For TEM characterization utilizing the multi-sample loading device, we loaded an Au standard, the synthetic HAp nanopowder, and the bone powder onto a single grid. We employed a half-mask method, which was accomplished *via* coating the Au standard on half of the grid area with a thickness of approximately 10 nm by using an ion coater (COXEM, KIC-1A). The synthetic HAp nanopowder was a commercial product (Aldrich, AL574791, 99.999%) that has a chemical composition of $Ca_5(PO_4)_3(OH)$ and an average

particle size of approximately 100 nm.[7,14] We obtained a bone sample from the femur of a three-year-old female *Bos taurus coreanae* (Gongju, South Korea) and cut the bone into a volume of 1.5 cm^3 with a precision saw (Buehler, Isomet 1000). The bone was milled using a freezer mill (SPEX, Freezer Mill 6700) for 5 min at a low temperature to minimize the alteration of the crystal structure during the milling process. Afterwards, the synthetic HAp and bone powders were separately diluted into ethanol, and each suspension was dropped onto a carbon-supported 300 mesh Cu grid (EMS Inc) using the multi-sample loading device to prevent cross-mixing of samples.

To image the boundary of the sample-loaded area prepared by the device, we used a scanning electron microscope (SEM; COXEM, CX-100) at 20 kV. The TEM characterization was performed with a side CCD camera (Olympus, Megaview III) attached to an energy-filtering TEM (Carl Zeiss, EM912Ω) at 120 kV. To investigate instrumental effects on structural analysis, ED patterns were acquired from a field emission TEM (JEOL, JEM-2100F) and a high voltage TEM (JEOL, JEM-ARM 1300S) at 200 kV and 1,250 kV, respectively. HRTEM images were obtained from the JEM-2100F. The program ELD[15] was used to correct the elliptical distortion and to obtain the intensity profiles of the ED patterns. XRD measurements of the synthetic HAp and bone powders were performed by using an XRD instrument (Bruker, D8 Advance) for the comparison of the d-spacing values. The 2θ range was from 5° to 145°, in steps of 0.02°, and the duration for each step was 2 s. The total time of analysis was approximately 4 h and 7,000 data points were obtained.

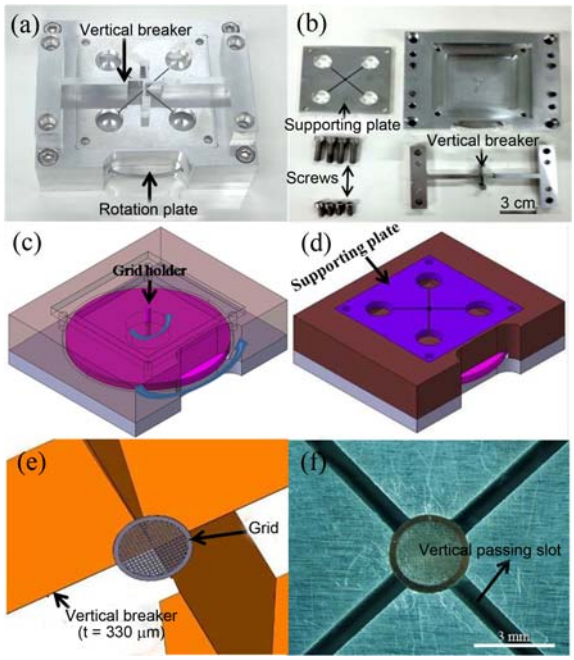

Figure 1. The Multi-sample loading device. (a) Complete features. (b) The device in its unassembled form. (c) Schematic image of the grid holder and rotation plate within the device. The grid is placed on top of the grid holder. (d) Schematic image of the device without the vertical breaker showing the supporting plate. (e) Ventral view of the grid being divided into four sections by the vertical breaker. (f) OM image of the grid placed on the grid holder after adjusting the holder to be slightly below the height (matching the thickness of the grid) of the supporting plate, prior to applying the vertical breaker.

Results and Discussion

Multi-sample Loading Device. Generally, one research sample is loaded on a TEM grid, but by using the multi-sample loading device, four research samples can be loaded on a single grid. This can be accomplished by using the vertical breaker of the device and by exploiting capillary forces. The device is made of aluminum alloy (AL6061) due to its ease of manufacturing with precise dimensional control and its durable property. The dimension of the device is 12.5 cm (W) × 10.4 cm (L) × 3.5 cm (H). When the vertical breaker is installed, the height is 4.5 cm. Figure 1(a) shows the image of the complete device, and Figure 1(b) shows the device in its unassembled state. The screws are used for adjusting the height of the supporting plate and vertical breaker. A schematic drawing of the interior of the device is shown in Figure 1(c). The rotation plate and grid holder (where a grid is placed on top of it) are comprised as a single unit, thus rotating simultaneously. The diameter of the grid holder is 3.05 mm, exactly matching the size (diameter) of the commercial grid. Figure 1(d) is a schematic drawing of the device with the vertical breaker removed, displaying the supporting plate. A single grid can be divided into 4 sections *via* the vertical breaker as shown in Figure 1(e). The thickness of the cross-shaped region of the vertical breaker is 330 μm on the front side where it meets the grid, and is 5 mm on the bottom side. After installing a grid to the holder of this device, the user can align the direction of the grid by adjusting the rotation plate. Through this process, the user can locate a position on the grid to load a sample for TEM analysis. Figure 1(f) is an optical microscopy (OM) image of the installed grid on the supporting plate. When the user loads a sample solution (nanopowder suspended in ethanol in this study) in each divided area of the grid with a pipette, the ethanol passes to the vertical slot (the diameter of each slot is 1 mm, and the depth is 5 mm) in the supporting plate. Therefore, by using the multi-sample loading device, a higher concentration of nanopowder can be achieved on the TEM grid as compared to more conventional methods because the ethanol is quickly removed.

Figure 2(a) is an OM image of a half-mask grid and designates the positions of the four samples on the grid. The half-mask method involved coating half the area (the darker section) of the grid with an internal standard, Au. Using the loading device, half the area, including both the coated and uncoated areas, was loaded with synthetic HAp, and the remaining half was loaded with bone powder. As a result, four separate sample sections were obtained on a single grid. Figure 2(b) is a SEM image of the boundary between the area coated with Au and uncoated sample area. It shows that the research samples are effectively blocked by the vertical breaker of the multi-sample loading device so that each

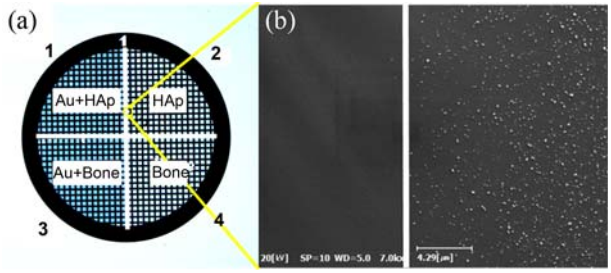

Figure 2. TEM grid prepared with loading device and half-mask method. (a) OM image of the grid half-coated with Au. Sample locations in each of the four sections and a selected section from the boundary area for SEM imaging are designated. (b) SEM image of boundary area shown in (a).

section is prevented from mixing with other sections. As a result, multiple research samples can be analyzed on a single grid *via* TEM under the same operation conditions.

TEM Characterization. As mentioned in the previous section, conventional internal standard methods have been applied for obtaining accurate structural information, particularly the d-spacing. However, these methods have limitations because of the vague image quality that originates from the high contrast of the standard material and the inaccurate intensity ratio from the overlapping of the ED patterns. These problems are resolved by using the half-mask method and by employing the multi-sample loading device. One section of the grid contains the research samples, and the other section contains both the internal standard and the research samples. The ED patterns of the internal standard and the research sample can be differentiated, enabling a more accurate peak analysis and d-spacing measurement. For applying different imaging techniques such as HRTEM and chemical or intensity-profile analysis of the ED pattern, the section without the internal standard can be used.

Figure 3 shows the BF-TEM images and the ED patterns of each section from a single grid. The images of the synthetic HAp and bone powders on the internal Au standard are blurred by the high contrast of the Au crystals. However, the particles on the amorphous carbon substrate are more easily observed. An individual synthetic HAp crystal has rectangular platelets, but the ED patterns of the HAp crystals display a spotty ring pattern without preferred orientations (Figure 3(b)). Such patterns are to be expected in the synthetic HAp considering the crystal type, size, and arrangement.[7,16] In the case of the bone powder, however, the bone-apatite nanocrystals appear to be aggregated. The ED pattern of the bone powder shows diffraction rings that include two diffuse territories, in contrast to that of the synthetic HAp. This is a result of the smaller sizes and lower crystallinity of the bone nanocrystals[16] as well as the organic materials in bone powder (Figure 3(d)).

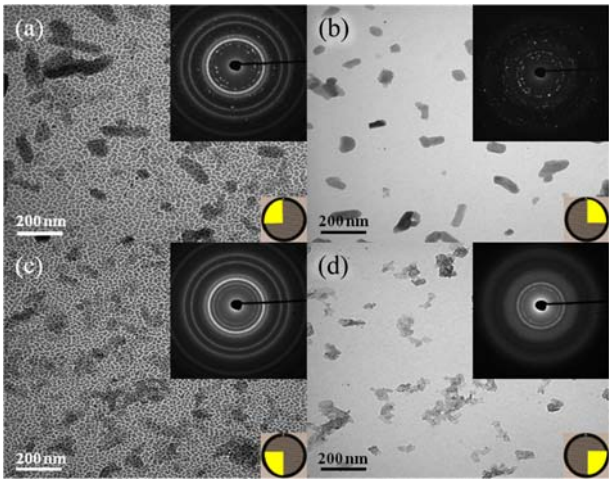

Figure 3. TEM analysis of grid prepared by multi-sample device. (a) Synthetic HAp on internal Au standard. (b) Synthetic HAp on normal carbon substrate. (c) Bone powder on internal Au standard. (d) Bone powder on normal carbon substrate.

Figure 4 shows the HRTEM images of the synthetic HAp and bone powders and their fast Fourier transform (FFT) patterns. The HRTEM image and FFT of synthetic HAp displays a single crystal structure and the crystal has rectangular platelets in which the c-axis is the elongated direction. On the other hand, the HRTEM image of the bone powder indicated that it appeared as if thin layers were stacked together. FFT pattern of the bone powder shows a textured pattern; the distribution of the {002} spots is similar to the previously reported ED patterns of bulk bone samples.[17-19] This indicates that the bone-apatite nanocrystals are directed along the *c*-axis, which may be due to the structural relationship between the bone-apatite nanocrystals and bone-related organic materials such as collagen.

Figure 5 displays the intensity profiles of the ED patterns acquired from each section using the ELD program.[15] The ED patterns from the internal standard area are influenced by the strong Au peaks (Figure 5(a)). Compared to intensity data from the amorphous carbon substrate area (Figure 5(b)), the {130} and {113} peaks (d_{130} = 2.26 Å, d_{113} = 2.06 Å)

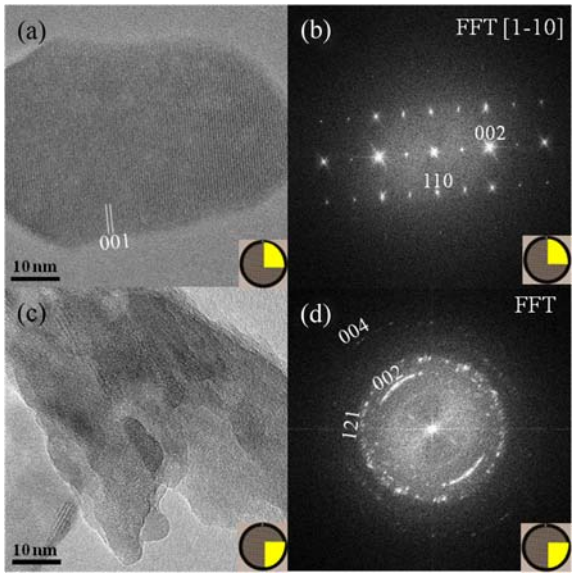

Figure 4. HRTEM images and their FFTs: (a) Synthetic HAp nanoparticle on normal carbon substrate; (b) FFT of (a); (c) Bone powder on carbon substrate; and (d) FFT of (c).

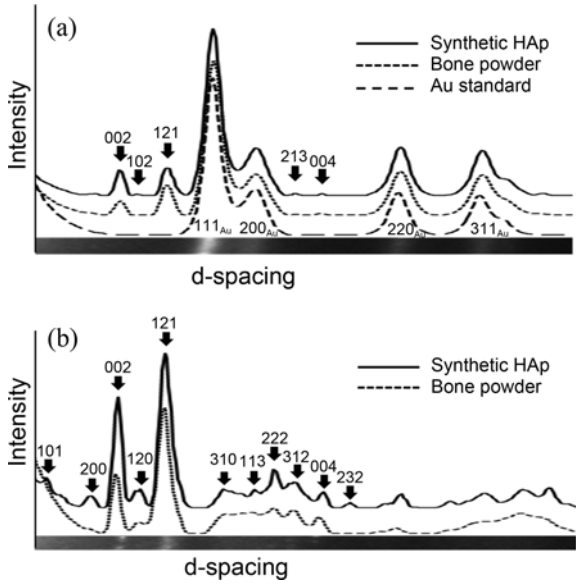

Figure 5. Intensity profiles of (a) ED data obtained from internal standard area and (b) ED data obtained from normal carbon substrate area.

from the synthetic HAp are obscured or blurred by the high intensity of the {111} and {200} peaks (d_{111} = 2.36 Å, d_{220} = 2.04 Å) from the Au standard. In general, the synthetic HAp displays sharper peaks compared to those of the bone powder, which indicates a larger crystal size and a higher crystallinity in the synthetic HAp nanocrystals.

To test the effectiveness of the internal standard method under different TEM operation conditions, the d-spacing values of two typical peaks, {002} and {121}, from the synthetic HAp were measured by using three TEM instruments, shown in Table 1. Based on the measurements using the EM912Ω, JEM-2100F, and JEM-ARM 1300S, ten ED patterns were obtained from each instrument. The precisions of d_{002} were 1.22%, 1.22%, and 0.75%, whereas those of d_{121} were 1.14%, 1.49%, and 0.71%, respectively. We were able to obtain a high level of precision regardless of the TEM operation conditions because the camera constant of each TEM instrument was corrected by calibrating the {111} ring of the Au internal standard (refer to Figure 5(a)). The {111} ring is the innermost and highest intensity ring of the Au diffraction ring pattern, and is effective as a calibration tool to minimize the errors of the d-spacing that originate from the Ewald curvature.[13,20] Referring to the experimental XRD data, the accuracy of the d-spacing was estimated for the EM912Ω, JEM-2100F, and JEM-ARM 1300S instruments. The accuracies of d_{002} were 0.03%, 0.09%, and 0.23%, whereas those of d_{121} were 0.11%, 0.36%, and 0.18%, respectively. Based on these d-spacing values, the accuracy of the lattice parameters were also estimated to be 0.12%, 0.42%, and 0.22%, respectively (refer to Table 1). The relatively large error in the JEM-2100F data originated from the smaller numbers of particles in the diffraction and their uneven sizes (40 to 240 nm).[7,21,22] Despite these shortcomings, the level of accuracy is significantly higher than that of the external standard method, which has an accuracy of approximately 2%; the accuracy is also higher than that of a conventional internal standard method and is affected less by the skills of the TEM operator.[12]

Conclusion

In this study, we fabricated four sample sections on a single grid by using a multi-sample loading device. To eliminate the disadvantages of previous internal standard methods, we applied a half-mask method, where half of the grid is coated with a standard material.

TEM characterization of the synthetic HAp and the bone powder was performed by employing the device with the internal standard method. We obtained high-quality images and reliable electron diffraction data from a single TEM grid.

The new device can reduce the TEM working time and increase the reliability of the TEM analysis of the nanomaterials by loading four different powder samples, including the internal standard, onto a single grid. The new device can be applied for the characterization of nanomaterials with similar structural and chemical properties, and the observation of morphological and structural changes in nanomaterials according to varying synthetic conditions.

Acknowledgments. We appreciate Sang-Gil Lee, Chang-Yeon Kim and Seung-Jo Yoo of the Korea Basic Science Institute for their technical support in the TEM analysis. This work was supported by a National Research Foundation of Korea grant funded by the Korean Government (MEST) (2012, University-Institute Cooperation Program).

Table 1. Results of structure determination using three different TEM instruments. Data from reference[14] and XRD experiments are listed for comparison

Synthetic HAp	d-spacing		Lattice parameters		
	d_{002} (Å)	d_{121} (Å)	a (Å)	c (Å)	a/c (Å)
XRD (ref.)	3.437	2.813	9.417(2)	6.875(2)	1.370
XRD (exp.)	3.437	2.806	9.391	6.874	1.366
EM912Ω (120 kV)	3.438 (21)	2.803 (16)	9.38	6.88	1.36
JEM-2100F (200 kV)	3.434 (21)	2.816 (21)	9.43	6.87	1.37
JEM-ARM 1300S (1250 kV)	3.445 (13)	2.801 (10)	9.37	6.89	1.36

References

1. Wiliams, D. B.; Carter, C. B. *Transmission Electron Microscopy*, 2nd ed.; Springer: New York, U.S.A., 2009; pp 3-22.
2. Malm, J. O.; O'Keefe, M. A. *Ultramicroscopy* **1997**, *68*, 13.
3. Champness, P. E. *Electron Diffraction in the Transmission Electron Microscope*; BIOS: United Kingdom, 2001; pp 1-23.
4. Stadelmann, P.; Leifer, K.; Verdon, C. *Ultramicroscopy* **1995**, *58*, 35.
5. Colella, M.; Lumpkin, G. R.; Zhang, Z.; Buck, E. C.; Smith, K. L. *Phys. Chem. Minerals* **2005**, *32*, 52.
6. Kim, J. G.; Seo, J. W.; Cheon, J.; Kim, Y. J. *Bull. Korean Chem. Soc.* **2009**, *30*, 183.
7. Song, K.; Kim, Y. J.; Kim, Y. I.; Kim, J. G. *J. Electron Microsc*. **2012**, *61*, 9.
8. Hammond, C. *The Basics of Crystallography and Diffraction*, 3nd ed.; Oxford University Press: United Kingdom, 2009; pp 243-273.
9. Grad, J. A. *Electron-optical Investigation of Clays*; Mineralogical Society: United Kingdom, 1971; pp 79-108.
10. Mugnaioli, E.; Capitani, G.; Nieto, F.; Mellini, M. *Am. Mineral.* **2009**, *94*, 793.
11. Lodder, J. C.; van der Berg, K. G. *J. Microsc.* **1974**, *100*, 93.
12. Schamp, C. T.; Jesser, W. A. *Ultramicroscopy* **2005**, *103*, 165.
13. Lee, Y. B.; Kim, Y. J. *Korean J. Microsc.* **1999**, *29*, 75.
14. Hughes, J. M.; Cameron, M.; Crowley, K. D. *Am. Mineral.* **1989**, *74*, 870.
15. Zou, X. D.; Sukharev, Y.; Hovmöller, S. *Ultramicroscopy* **1993**, *49*, 147.
16. Suvorova, E. I.; Buffat, P. A. *J. Microscopy* **1999**, *196*, 46.
17. Su, X.; Sun, K.; Cui, F. Z.; Landis, W. J. *Bone* **2003**, *32*, 150.
18. Wenk, H. R.; Heidelbach, F. *Bone* **1999**, *24*, 361.
19. Olszta, M. J.; Cheng, X.; Jee, S. S.; Kumar, R.; Kim, Y. Y.; Kaufman, M. J.; Douglas, E. P.; Gower, L. B. *Mater. Sci. Eng.* **2007**, *R58*, 77.
20. Lee, S. G.; Song, K.; Kim, J. G. *Korean J. Microsc.* **2011**, *41*, 75.
21. Prevéy, P. S. *J. Therm. Spray Technol*. **2000**, *9*, 369.
22. Gibbs, R. J. *Am. Mineral*. **1965**, *50*, 741.